Journal Pre-proof

Cav3.2 T-type calcium channel mediates acute itch and contributes to chronic itch and inflammation in experimental atopic dermatitis

Ji-Woong Ahn, M.S, Song-Ee Kim, M.S., Do-Young Kim, M.D., Ph.D., Inhye Jeong, M.S., Sohyun Kim, M.D., Seungsoo Chung, M.D., Ph.D., Sang Eun Lee, M.D., Ph.D.

PII: S0022-202X(23)02919-6

DOI: https://doi.org/10.1016/j.jid.2023.07.029

Reference: JID 4016

To appear in: *The Journal of Investigative Dermatology*

Received Date: 20 January 2023

Revised Date: 21 June 2023

Accepted Date: 24 July 2023

Please cite this article as: Ahn J-W, Kim S-E, Kim D-Y, Jeong I, Kim S, Chung S, Lee SE, Cav3.2 T-type calcium channel mediates acute itch and contributes to chronic itch and inflammation in experimental atopic dermatitis, *The Journal of Investigative Dermatology* (2023), doi: https://doi.org/10.1016/j.jid.2023.07.029.

Original Article

Cav3.2 T-type calcium channel mediates acute itch and contributes to chronic itch and inflammation in experimental atopic dermatitis

Ji-Woong Ahn, M.S[1,4], Song-Ee Kim, M.S.[2,4], Do-Young Kim, M.D., Ph.D.[3], Inhye Jeong, M.S.[2], Sohyun Kim, M.D.[1], Seungsoo Chung, M.D., Ph.D.[1,5], Sang Eun Lee, M.D., Ph.D.[2,5]

[1]*Brain Korea 21 Plus Project for Medical Science, Department of Physiology, Yonsei University College of Medicine, Seoul 03722, Republic of Korea;*

[2]*Department of Dermatology and Cutaneous Biology Research Institute, Gangnam Severance Hospital, Yonsei University College of Medicine, Seoul, Korea.*

[3]*Department of Dermatology and Cutaneous Biology Research Institute, Severance Hospital, Yonsei University College of Medicine, Seoul, Korea.*

[4]These authors contributed equally to this work.

[5]These authors contributed equally to this work.

ORCIDs

Ji-Woong Ahn: https://orcid.org/0000-0001-6951-5422

Song-Ee Kim: https://orcid.org/0000-0001-7369-7310

Do-Young Kim: http://orcid.org/0000-0002-0194-9854

Inhye Jeong: https://orcid.org/0000-0002-7458-1464

Sohyun Kim: https://orcid.org/0000-0003-0820-3411

Seungsoo Chung: https://orcid.org/0000-0002-3119-9628

Sang Eun Lee: https://orcid.org/0000-0003-4720-9955

Correspondence: Sang Eun Lee, Department of Dermatology, Gangnam Severance Hospital, Yonsei University College of Medicine, 211 Eonjuro, Gangnam-gu, Seoul 06273, Korea, Tel.: 82-2-2019-3360, Fax: 82-2-3463-6136, E-mail: jennifer823@yuhs.ac or Seungsoo Chung, Department of Physiology, Yonsei University College of Medicine, Seoul 03722, Republic of Korea, E-mail: SSCHUNG@yuhs.ac

Short title: Cav3.2 in acute and chronic itch

Abbreviations: AD, atopic dermatitis; CGRP, calcitonin gene-related peptide; DRG, dorsal root ganglion; IL-4Rα, interleukin-4 receptor α; IL-13Rα1, IL-13 receptor α1; LTMRs, low-threshold mechanoreceptors; NF, neurofilament; NP, non-peptidergic; PAR2-AP, protease-activated receptor-2 agonist peptide; PEP, peptidergic; rm, recombinant mouse; scRNA-seq, single cell RNA-sequencing; T-currents , T-type calcium current; TG, trigeminal ganglia; TH, tyrosine hydroxylase; TRP, transient receptor potential; TSLP, thymic stromal lymphopoietin receptor; tSNE, t-distributed stochastic neighbor embedding; TTCC, T-type calcium channel; VIP, vasoactive intestinal polypeptide; WT, wild-type

ABSTRACT

Voltage-gated calcium channels regulate neuronal excitability. The Cav3.2 isoform of the T-type voltage-activated calcium channel is expressed in sensory neurons and is implicated in pain transmission. However, its role in itch remains unclear. Herein, we demonstrated that Cav3.2 is expressed by mechanosensory and peptidergic subsets of mouse dorsal root ganglion (DRG) neurons and colocalized with TRPV1 and receptors for type 2 cytokines. Cav3.2-positive neurons innervate human skin. A deficiency of Cav3.2 reduces histamine, IL-4/IL-13, and thymic stromal lymphopoietin-induced itch in mice. Cav3.2 channels were upregulated in the DRGs of an atopic dermatitis (AD)-like mouse model and mediated neuronal excitability. Genetic knockout of Cav3.2 or T-type calcium channel blocker mibefradil treatment reduced spontaneous and mechanically induced scratching behaviors and skin inflammation in an AD-like mouse model. Substance P and vasoactive intestinal polypeptide levels were increased in the trigeminal ganglia (TG) from AD-like mouse model, and genetic ablation or pharmacological inhibition of Cav3.2 reduced their gene expression. Cav3.2 knockout also attenuated the pathologic changes in *ex vivo* skin explants co-cultured with TG neurons from AD-induced mice. Our study identifies the role of Cav3.2 in both histaminergic and non-histaminergic acute itch. Cav3.2 channel also contributes to AD-related chronic itch and neuroinflammation.

Key words: Cav3.2, T-type voltage-activated calcium channel, itch, atopic dermatitis, substance P, vasoactive intestinal polypeptide, neuroinflammation

INTRODUCTION

Itch is a common symptom in many skin diseases, systemic disorders, and neuropathic disorders. The complexity and redundancy of itch signaling pathways make medical control of itch unsatisfactory.

Many itch mediators bind to G protein-coupled receptors on sensory neurons, activating transient receptor potential (TRP) channels to cause voltage changes. This activates voltage-gated ion channels, generating and propagating action potentials (Kittaka and Tominaga, 2017).

Nav1.7- Nav1.9, the subtypes of voltage-gated sodium channels, are known to be involved in itch sensation (Kühn et al., 2020, Lee et al., 2014). In addition to sodium ions, calcium is also critically involved in neuronal excitability. Calcium influx via voltage-gated calcium channels not only controls membrane excitability, but also regulates gene transcription and neurotransmitter release (Berridge, 2006, Neher and Sakaba, 2008, Simms and Zamponi, 2014). Voltage-gated calcium channels are classified into high voltage-activated L, N, P/Q, and R-type and low voltage-activated T-type channels. T-type calcium channels (TTCC) are key regulators of neuronal excitability because they are activated by small depolarization and induce low-threshold action potential initiation (Nelson et al., 2005, Nelson et al., 2007).

Among the TTCCs (Cav3), Cav3.2 is the major isoform that is abundantly expressed in small and medium-diameter nociceptors (François et al., 2015, Rose et al., 2013). Immunohistochemical studies have shown that mouse dorsal root ganglia (DRG) neurons immunoreactive to Cav3.2 co-expressed both nonpeptidergic and peptidergic nociceptor markers, isolectin B4 and calcitonin gene-related peptide (CGRP), respectively (Rose et al., 2013). Cav3.2 channels were also found in Aδ-and C-fiber-associated cutaneous low-threshold mechanoreceptors (LTMRs) (François et al., 2015). However, the precise

distribution of Cav3.2 channels in peripheral sensory neurons remains unclear.

Cav3.2 channels are well-known to play an important role in pain transmission (Bourinet et al., 2005, Choi et al., 2007, Francois et al., 2013) and are upregulated in DRGs in various inflammatory and neuropathic pain models (Jagodic et al., 2008, Marger et al., 2011). However, the role of Cav3.2 in itch is not well understood. Few studies have examined Cav3.2's role in acute itch (Gadotti et al., 2020, Lin et al., 2017, Wang et al., 2015). Pharmacological inhibition of TTCCs or Cav3.2 silencing in the spinal cord reduces hydrogen sulfide-induced scratching in mice (Wang et al., 2015). Cav3.2 knockout or TTCCs blocker has been shown to reduce histamine and chloroquine-induced scratching (Gadotti et al., 2020). In another study, a pan-TTCCs blocker reduced chloroquine-, endothelin-1-, and histamine-induced itch; however, zinc, an another TTCCs antagonist, did not show the same effect (Lin et al., 2017). Chronic itch is a highly burdensome condition and is most often caused by inflammatory skin diseases, including atopic dermatitis (AD). However, the role of Cav3.2 in chronic itch remains unexplored.

In this study, we analyzed a public dataset of single-cell transcriptomes of mouse DRGs to define subpopulations of Cav3.2-expressing neurons and investigated a role of Cav3.2 channel in various pruritogens-evoked acute itch. We also explored the role of Cav3.2 in chronic itch, neuropeptide production and skin inflammation using a mouse model of AD.

RESULTS

Cav3.2 channel is co-expressed with TRPV1, IL-4Rα, and TSLP receptor in peptidergic subsets of mouse DRGs

First, we examined the expression and distribution of Cav3.2 channels in mouse DRG neurons. As shown in Figure 1a, Cav3.2 immunoreactivity was detected in a subset of DRG neurons from C57BL/6 wild-type (WT) mice, but was undetectable in Cav3.2 knockout mice. Then, we reanalyzed a published dataset of single-cell transcriptional profiling of the adult mouse nervous system (Zeisel et al., 2018) to identify molecularly defined subpopulations of Cav3.2-expressing neurons.

After dimensional reduction analysis of 153,633 cells that were filtered based on mito gene < 20%, 24 clusters were recognized using t-distributed stochastic neighbor embedding (tSNE) dimensionality reduction. We identified a population of peripheral sensory neurons (cluster 14) based on the markers of pruriceptors including Mas-related G-protein-coupled receptor (Mrgpr)A3 and natriuretic polypeptide B (Nppb) (Dong and Dong, 2018) (Figure 1b and c). Using the known cell-type markers, we identified four main clusters within the peripheral sensory neurons, including i) non-peptidergic (NP) clusters (NP 1, NP2, and NP3, which expressed MrgprD, MrgprA3, and Nppb transcripts, respectively), ii) peptidergic (PEP) clusters that expressed *Tac1* (substance P) and *Calca* (CGRP), iii) tyrosine hydroxylase (TH)-expressing cluster, which highly expressed the mechanosensory channel PIEZO2 gene, and iv) *Nefh* (neurofilament heavy chain)-expressing neurofilament (NF) cluster (Figure 1d), based on the recent classification of mouse DRG neurons (Usoskin et al., 2015). We found that Cav3.2 transcript (*Cacna1h*) is expressed in NF and TH clusters, which are lightly myelinated Aδ nociceptors and C-LTMRs, respectively, consistent with previous findings (François et al., 2015). Cav3.2 transcripts were scarcely detected in the NP clusters, however they were widely distributed in the PEP clusters. Unlike Cav3.2, Cav3.1 (*Cacna1g*) and Cav3.3 (*Cacna1i*) transcripts were restricted to TH and NF clusters. In PEP neurons, the expression of Cav3.2 transcripts overlapped with that of *Il4ra* (interleukin-4 receptor α, IL-

4Rα), *Il13ra1* (IL-13 receptor α1, IL-13Rα1), and *Crlf2* (thymic stromal lymphopoietin [TSLP] receptor), which broadly spanned NP and PEP neurons (Oetjen et al., 2017). *Trpv1* (TRP vanilloid 1, TRPV1) was highly expressed in PEP neurons and largely overlapped with Cav3.2 transcripts (Figure 1d).

Double immunofluorescence staining revealed that 47.4% of CGRP-expressing DRG neurons and 35% of TRPV1+ neurons co-expressed Cav3.2. Additionally, Cav3.2 immunoreactivity was detected in 56.1% of IL-4Rα+ neurons and 53.3% of TSLP receptor+ neurons (Figures 1e and f). The specificity of antibodies was confirmed by negative control staining without primary antibodies (Supplementary Figure S1). These findings suggest that Cav3.2 channels are expressed not only in LTMRs, but also in a subset of peptidergic C-fibers and colocalized with TRPV1, IL-4Rα, and TSLP receptor.

Cav3.2 channels are present in peripheral nerve fibers in human skin

To examined whether Cav3.2 channels are present in distal peripheral nerves located in human skin, we performed double immunofluorescence staining for Cav3.2 and PGP9.5, a pan-neuronal marker. As demonstrated in Figure 2, subepidermal neural plexus and epidermal nerve fibers that exhibited PGP9.5 labeling were also strongly immunolabeled with Cav3.2 in normal human skin, suggesting that Cav3.2 channels are expressed in the peripheral nerve terminals.

Cav3.2 channel mediates acute itch response induced by histamine, TSLP, and IL-4/IL-13

Next, we investigated whether Cav3.2 is involved in known pruritogens-induced acute itch. Intradermal cheek injections of histamine, chloroquine, protease-activated receptor-2 agonist peptide (PAR2-AP), recombinant mouse (rm) TSLP, rmIL-31, or a combination of rmIL-4 and

rmIL-13 (rmIL-4/IL-13) induced scratching behavior in WT mice. Pretreatment with a pan-TTCCs blocker, mibefradil, significantly attenuated histamine-, rmTSLP- or rmIL-4/IL-13-induced scratching bouts. Chloroquine-induced scratching showed a tendency to decrease with mibefradil treatment; however, these changes did not reach statistical significance (P=0.056) (Figure 3a). Then, we utilized Cav3.2 knockout mice to verify the role of Cav3.2 isoform in acute itch. Consistent with the results obtained using mibefradil, histamine-, rmTSLP-, or rmIL-4/IL-13-induced scratching was reduced in Cav3.2 knockout mice than in WT mice. However, chloroquine-, PAR2-AP-, and rmIL-31-induced scratching was not significantly altered in Cav3.2 knockout mice (Figure 3b).

Cav3.2 channels are upregulated and contribute to increased excitability of DRG neurons in the MC903-induced AD-like mouse model

To assess the role of Cav3.2 in chronic itch in AD, we used a MC903-induced AD-like mouse model (Li et al., 2006). First, we examined the expression and function of Cav3.2 channels in the DRG neurons of MC903-induced experimental AD. Daily application of MC903 (calcipotriol) to the cheek and nape of the neck of C57BL/6 mice induced skin thickening, erythema, and scales accompanied by spontaneous scratching behavior (Figure 4a, 5a, 6a). Immunofluorescence analysis and real-time RT-PCR revealed increased immunoreactivity and mRNA levels of Cav3.2 in the DRGs of MC903-treated mice compared to vehicle-treated mice (Figure 4b). Using a whole-cell patch-clamp, we found an upregulated T-type calcium current (T-currents) density (pA/pF) in DRG neurons from MC903-treated mice compared to that in vehicle-treated controls (Figure 4c). Topical and intradermal administration of mibefradil to mice while eliciting MC903-induced AD (Figure 4a) resulted in a reduction in T-currents (Figure 4c). To investigate the contribution of Cav3.2 in this increase in T-currents,

we challenged Cav3.2 knockout mice with experimental AD (Figure 4a). Cav3.2 knockout decreased T-currents in DRG neurons from MC903-treated mice (Figure 4c), suggesting an increased activity of Cav3.2 channels in DRG neurons of MC903-AD mice.

To directly investigate the effect of MC903-induced atopic inflammation on the excitability of DRG neurons, we determined the firing frequency of action potentials in DRG neurons after MC903 treatment. Injection of positive currents induced action potentials in vehicle-treated murine DRG neurons in a stimulus-dependent manner. The action potential firing rate was significantly increased in DRG neurons from MC903-treated mice compared to vehicle-treated controls at all current ranges tested (Figure 4d). Additionally, the action potential threshold of DRG neurons was decreased in MC903-treated mice (Figure 4e), suggesting that MC903-induced AD-like inflammation increased neuronal excitability. To investigate the contribution of Cav3.2 channels, we evaluated the effect of pharmacological inhibition of Cav3.2 on DRG neurons of MC903-AD mice. Administration of mibefradil to MC903-AD mice resulted in a significant reduction in action potential firing rate (Figure 4d) and an increase in the action potential threshold by 59% in DRG neurons (Figure 4e). We next examined the functional consequences of Cav3.2 knockout in neuronal excitability in MC903-treated DRG neurons. The action potential firing rate in these neurons was significantly reduced and the action potential threshold was increased by 61% in Cav3.2 knockout mice than in the control littermates when challenged with MC903 (Figure 4d and e). These results indicate that the increased neuronal excitability observed in MC903-treated AD mice is dependent on Cav3.2 channels.

Cav3.2 channel plays an important role in chronic itch and alloknesis in MC903-induced AD model

Then, we studied the effects of Cav3.2 knockout or pharmacological inhibition of TTCCs on scratching behavior of MC903-treated mice. Increased scratching behavior in MC903-treated mice was attenuated by administration of mibefradil (Figure 5a). Cav3.2 knockout mice also displayed a significant reduction in scratching behavior compared to littermate controls upon induction of AD-like disease (Figure 5b), indicating the involvement of the Cav3.2 channel in chronic itch associated with AD-like inflammation.

Since Cav3.2 channels are expressed in mechanoreceptors, we subsequently examined their role in alloknesis. Von Frey stimulation did not induce scratch responses in vehicle-treated controls but elicited scratch bouts in MC903-treated mice. The von Frey stimulation-evoked scratch response in MC903-treated mice was abolished by the administration of mibefradil (Figure 5c). Moreover, Cav3.2 knockout also inhibited the von Frey stimulation-induced scratch response in MC903-AD mice (Figure 5d).

Cav3.2 deficiency alleviates skin inflammation and reduces the production of substance P and VIP from TG neurons in MC903-induced AD-like mice

Peptidergic nerves modulate cutaneous immunity via regulating the release of neuropeptides. Given our finding of Cav3.2 expression in TRPV1+ peptidergic neurons, we hypothesized that Cav3.2 may influence skin inflammation in experimental AD. Interestingly, erythema and scaling of AD-induced mice co-treated with mibefradil were less than those in the vehicle control mice (Figure 6a). The administration of mibefradil significantly reduced the MC903-induced increase in epidermal thickening, dermal infiltration of inflammatory cells, including mast cells, and the mRNA expression levels of IL-13, IL-4, and TSLP in the lesional skin (Figure 6b-d). When investigating the effects of mibefradil at different doses on the skin phenotypes of MC903-treated mice, we observed a more pronounced reduction in scaling and

epidermal thickness at the higher doses of 15 μg/20 μl and 35 μg/20 μl compared to the lower dose of 1.2 μg/20 μl. Additionally, we observed significant reductions in the mRNA levels of IL-13 and IL-4 only at doses higher than 15 μg/20 μl (Supplementary Figure S2).

Cav3.2 knockout mice also exhibited, although to a lesser extent, a reduced atopic phenotype when challenged with MC903 compared to littermate controls (Figure 6a). Knockout of Cav3.2 attenuated MC903-induced epidermal thickness and infiltration of inflammatory cells, including mast cells (Figure 6b and c). The increase in IL-5, IL-13, IL-4, and TSLP mRNA levels in the lesional skin of Cav3.2 knockout mice was lower than that in littermate controls upon induction of AD-like disease (Figure 6d). These results indicate a role of Cav3.2 in the development of MC903-induced AD-like inflammation.

To elucidate the possible mechanism by which Cav3.2 channel inhibition affects skin phenotype, we first examined Cav3.2 expression in keratinocytes. Real-time PCR and western blot analysis confirmed that Cav3.2 was barely detected in mouse keratinocytes (Supplementary Figure S3). We next investigated whether Cav3.2 deficiency alters the expression of neuropeptides in trigeminal ganglia (TG) neurons from MC903-AD mice. We screened nine neuropeptide-encoding genes including *Calca*, *Tac1*, *Tac2* (neurokinin B), *Vip* (vasoactive intestinal polypeptide, VIP), *Adcyap1* (pituitary adenylate cyclase-activating polypeptide), *Nppb*, *Npy* (Neuropeptide Y), *Nmu* (Neuromedin U), and *Nts* (neurotensin), which have been reported to be produced by DRGs and TGs (Chen, 2021). Among these, the mRNA expression of *Tac1*, *Tac2*, and *Vip* increased in the TGs from MC903-treated mice (Figure 6e). Notably, MC903-treated Cav3.2 knockout mice showed decreased expression of *Tac1* and *Vip* in TGs compared to littermate controls. The upregulation of *Tac1* and *Vip* transcripts in the TGs of MC903-AD mice was also attenuated by mibefradil treatment (Figure 6f), indicating that Cav3.2 regulates substance P and VIP expression in sensory neurons during

the development of experimental AD. To further investigate the specific role of neuronal Cav3.2 in skin inflammation, we utilized an *ex vivo* co-culture model comprising normal mouse skin explants and TG neurons from MC903-treated WT or Cav3.2 knockout mice. Substance P and VIP levels in the culture medium of TGs from MC903-treated WT mice increased; however, this increase was attenuated in the culture medium of TGs from MC903-treated Cav3.2 knockout mice (Supplementary Figure S4a). Additionally, the skin explants co-cultured with TGs from MC903-treated WT mice showed increased dermal inflammatory infiltrates, epidermal thickening, and transcription of IL-4 and IL-5. Conversely, these increases were attenuated in the skin explants co-cultured with TGs from MC903-treated Cav3.2 knockout mice (Supplementary Figure S4b-d). Together, these results suggest that Cav3.2 in TG neurons might modulate skin inflammation in MC903-treated AD-like model.

DISCUSSION

Our study demonstrates the involvement of Cav3.2, the major isoform of TTCCs, in histaminergic and type 2 cytokines-associated non-histaminergic acute itch. Through the use of Cav3.2 knockout mice and a pharmacological approach, we also demonstrated the role of Cav3.2 channels in chronic itch and alloknesis in the MC903-induced AD-like mouse model. Through immunofluorescence studies and analysis of single cell RNA-sequencing (scRNA-seq) datasets of mouse neurons (Usoskin et al., 2015, Zeisel et al., 2018), we found that Cav3.2 is expressed in subsets of peptidergic neurons as well as Aδ- and C-LTMRs, as previously reported (François et al., 2015). Cav3.2 transcripts scarcely overlapped with markers of non-peptidergic neurons. Additionally, we demonstrated that Cav3.2 transcripts coexisted with TRPV1 and receptors for type 2 cytokines, IL-4Rα and TSLP receptor, in peptidergic neurons. Furthermore, we detected the expression of Cav3.2 channels in the peripheral nerve terminals within human

skin, suggesting their involvement in peripheral itch pathways.

These observations are in line with the findings from our *in vivo* acute itch assay. Consistent with previous report (Gadotti et al., 2020), we confirmed that Cav3.2 mediates histamine-induced itch, which is known to be mediated by TRPV1. We also demonstrated a role of Cav3.2 in acute itch response evoked by TSLP or IL-4/IL-13, but not PAR2-AP or IL-31. Although Cav3.2 knockout did not significantly affect chloroquine-induced scratching, there was a tendency for a reduction observed with mibefradil treatment (p=0.056). This difference might be attributed to the pharmacological properties of mibefradil, a pan-TTCCs inhibitor rather than a selective inhibitor of the Cav3.2 isoform (Martin et al., 2000).

Type 2 cytokines are also implicated in non-histaminergic chronic itch in AD. In the MC903-induced AD-like mouse model, we found the increased expression and activity of Cav3.2 channels in DRG neurons. Increased frequencies of action potential firing and decreased action potential threshold in DRGs of the MC903-AD model were attenuated by Cav3.2 deficiency, indicating a contribution of Cav3.2 to increased neuronal excitability. Increasing TTCCs expression has been shown to decrease the threshold for action potential firing in primary afferent neurons (Jagodic et al., 2007, Li et al., 2017), consistent with our findings. We also demonstrated that Cav3.2 knockout or mibefradil treatment significantly decreased chronic spontaneous scratching in MC903-AD mice. Taken together, Cav3.2 channels are upregulated in primary sensory neurons under atopic conditions and contribute to neuronal excitability and chronic itch.

Additionally, Cav3.2 deficiency reduced light touch-induced scratching responses in MC903-AD model, suggesting a role of Cav3.2 in AD-associated alloknesis. Patients with AD often experience alloknesis, but the underlying mechanisms are unknown. Aβ-LTMRs have been proposed to mediate alloknesis (Pan et al., 2019, Sakai and Akiyama, 2020). Moreover, C-

LTMRs expressing Cav3.2 contribute to mechanical and cold allodynia in peripheral neuropathy (François et al., 2015). Together, the increased activity of Cav3.2 channels in Aδ- or C-LTMRs may contribute to alloknesis in AD.

Interestingly, Cav3.2 knockout or treatment with mibefradil alleviated the skin phenotype of the MC903-AD model, accompanied by decreased mast cell infiltration and Th2 cytokines transcripts in the skin, suggesting a role of Cav3.2 not only in chronic itch but also in the development of AD-like inflammation. It is possible that the reduction in scratching resulting from Cav3.2 inhibition might lead to alleviation of dermatitis by preventing secondary skin damage. However, by utilizing an *ex vivo* co-culture model, we found that the TG neurons from MC903-treated mice directly induced pathologic changes in the skin explants, including increased epidermal thickness, inflammatory infiltrates, and transcription of IL-4 and IL-5. Notably, these changes were attenuated in skin explants co-cultured with TG neurons from MC903-treated Cav3.2 knockout mice, suggesting a role of neuronal Cav3.2 in skin inflammation. Through neuropeptide screening, we also demonstrated that Cav3.2 is involved in the increased production of substance P and VIP from TG neurons in MC903-treated mice. Substance P and VIP released from nociceptors elicit allergic inflammation by activating inflammatory cells including mast cells and eosinophils (Nakashima et al., 2019). Taken together, our data suggest that neuronal Cav3.2 might modulate MC903-induced AD-like inflammation, potentially by regulating neuronal production of substance P and VIP. Regarding the expression of Cav3 channels in skin components other than nerves, Cav3.1 isoform is implicated in the function of Th2 and Th17 cells, whereas the transcription of Cav3.2 and Cav3.3 has been reported to occur in an incomplete form, suggesting the possibility of their nonfunctional presence in T cells (Erdogmus et al., 2022). Therefore, it is unlikely that Cav3.2 knockout affects the function of T lymphocytes. However, mibefradil, a

broad-spectrum TTCCs blocker, may inhibit Cav3.1 channels in T cells and potentially suppress inflammatory responses in the skin. These findings can partially explain why mibefradil administration was more effective than Cav3.2 knockout in reducing the MC903-induced skin phenotype.

In conclusion, our study provides evidence that Cav3.2 channels in a subset of peptidergic neurons are involved in the acute itch pathways mediated by histamine, IL-4/13, or TSLP. Furthermore, we demonstrated that under AD-like inflammatory conditions, upregulated Cav3.2 channels in sensory neurons not only contribute to chronic itch but also play a role in neuroinflammation. These findings highlight the potential of Cav3.2 as a therapeutic target for both acute histaminergic itch and the chronic itch and inflammation associated with AD.

MATERIALS AND METHODS

Animals

C57BL/6 mice and Cana1h-/- (Cav3.2 knockout) mice were obtained from the Jackson Laboratory (Bar Harbor, ME, USA). Cana1h-/- mice (Jackson Laboratory, #013770) were maintained on a C57BL/6J background in our laboratory, housed under constant day/night cycles, with a room temperature of 22 °C, and provided food and water ad libitum. The Institutional Animal Care and Use Committee of Yonsei University approved all animal protocols utilized here. Age-matched littermate mice (Cav3.2+/+ mice) were used as controls. Cav3.2+/− mice were excluded from this study.

MC903-induced experimental AD and drug administration

To induce AD-like mouse model, we applied MC903 (R&D Systems, Minneapolis, MN) to the cheek and neck (0.2 mM in 20 μl ethanol [vehicle]) of age-matched C57BL/6 mice

(Cav3.2+/+) and Cana1h-/- mice (12 weeks old) once daily for 9 days (day 0–8). Control mice were treated with 20 μl ethanol. On day 9, spontaneous scratching behavior and alloknesis were evaluated. TGs, eight cervical DRGs, and lesional skin tissues were obtained for qRT-PCR, immunofluorescence, and immunohistochemistry. For pharmacological inhibition of TTCCs, mibefradil (15 μg /20 μl) was administered topically for 2 days (days 3-4) and intradermally for 4 days (days 5-8) during the development of AD with MC903. The control group underwent the same experimental procedures with vehicle (phosphate-buffered saline).

Data analysis

Statistical analysis was performed using GraphPad Prism 6 software (GraphPad Software, Inc, La Jolla, CA). P <0.05 was considered to indicate a statistically significant difference. A two-tailed unpaired Student′s t-test was used to compare the data between two groups.

Details of all experimental procedures are described in Supplementary Materials and Methods.

Data availability statement

No datasets were generated during this study. All data analyzed during this study are included in this published article and its supplementary information files.

Conflict of Interest

The authors state no conflict of interest.

Acknowledgments

This research was supported by grants from the National Research Foundation of Korea (NRF) (no. 2018R1C1B6005644).

Author contributions

Conceptualization: SEL, SC; Funding Acquisition: SEL; Investigation: JWA, SEK, IJ, SK; Formal analysis: DYK; Writing – Original Draft Preparation: SEL, SK; Writing – Review and Editing: SC

Reference

Berridge MJ. Calcium microdomains: organization and function. Cell calcium 2006;40(5-6):405-12.

Bourinet E, Alloui A, Monteil A, Barrere C, Couette B, Poirot O, et al. Silencing of the Cav3. 2 T-type calcium channel gene in sensory neurons demonstrates its major role in nociception. The EMBO journal 2005;24(2):315-24.

Chen Z-F. A neuropeptide code for itch. Nature Reviews Neuroscience 2021;22(12):758-76.

Choi S, Na H, Kim J, Lee J, Lee S, Kim D, et al. Attenuated pain responses in mice lacking CaV3. 2 T-type channels. Genes, Brain and Behavior 2007;6(5):425-31.

Dong X, Dong X. Peripheral and central mechanisms of itch. Neuron 2018;98(3):482-94.

Erdogmus S, Concepcion AR, Yamashita M, Sidhu I, Tao AY, Li W, et al. Cavβ1 regulates T cell expansion and apoptosis independently of voltage-gated Ca2+ channel function. Nat Commun 2022;13(1):2033.

Francois A, Kerckhove N, Meleine M, Alloui A, Barrere C, Gelot A, et al. State-dependent properties of a new T-type calcium channel blocker enhance CaV3. 2 selectivity and support analgesic effects. Pain 2013;154(2):283-93.

François A, Schüetter N, Laffray S, Sanguesa J, Pizzoccaro A, Dubel S, et al. The low-threshold calcium channel Cav3. 2 determines low-threshold mechanoreceptor function. Cell reports 2015;10(3):370-82.

Gadotti VM, Kreitinger JM, Wageling NB, Budke D, Diaz P, Zamponi GW. Cav3. 2 T-type calcium channels control acute itch in mice. Molecular Brain 2020;13(1):1-7.

Jagodic MM, Pathirathna S, Joksovic PM, Lee W, Nelson MT, Naik AK, et al. Upregulation of the T-type calcium current in small rat sensory neurons after chronic constrictive injury of the sciatic nerve. Journal of neurophysiology 2008;99(6):3151-6.

Jagodic MM, Pathirathna S, Nelson MT, Mancuso S, Joksovic PM, Rosenberg ER, et al. Cell-specific alterations of T-type calcium current in painful diabetic neuropathy enhance excitability of sensory neurons. Journal of Neuroscience 2007;27(12):3305-16.

Kittaka H, Tominaga M. The molecular and cellular mechanisms of itch and the involvement of TRP channels in the peripheral sensory nervous system and skin. Allergology International 2017;66(1):22-30.

Kühn H, Kappes L, Wolf K, Gebhardt L, Neurath MF, Reeh P, et al. Complementary roles of murine NaV1. 7, NaV1. 8 and NaV1. 9 in acute itch signalling. Scientific reports 2020;10(1):1-12.

Lee J-H, Park C-K, Chen G, Han Q, Xie R-G, Liu T, et al. RETRACTED: A Monoclonal Antibody that Targets a NaV1. 7 Channel Voltage Sensor for Pain and Itch Relief. Elsevier; 2014.

Li M, Hener P, Zhang Z, Kato S, Metzger D, Chambon P. Topical vitamin D3 and low-calcemic analogs induce thymic stromal lymphopoietin in mouse keratinocytes and trigger an atopic dermatitis. Proceedings of the National Academy of Sciences 2006;103(31):11736-41.

Li Y, Tatsui CE, Rhines LD, North RY, Harrison DS, Cassidy RM, et al. Dorsal root ganglion neurons become hyperexcitable and increase expression of voltage-gated T-type calcium channels

(Cav3. 2) in paclitaxel-induced peripheral neuropathy. Pain 2017;158(3):417.

Lin S-F, Wang B, Zhang F-M, Fei Y-H, Gu J-H, Li J, et al. T-type calcium channels, but not Cav3. 2, in the peripheral sensory afferents are involved in acute itch in mice. Biochemical and Biophysical Research Communications 2017;487(4):801-6.

Marger F, Gelot A, Alloui A, Matricon J, Ferrer JFS, Barrère C, et al. T-type calcium channels contribute to colonic hypersensitivity in a rat model of irritable bowel syndrome. Proceedings of the National Academy of Sciences 2011;108(27):11268-73.

Martin RL, Lee J-H, Cribbs LL, Perez-Reyes E, Hanck DA. Mibefradil block of cloned T-type calcium channels. Journal of Pharmacology and Experimental Therapeutics 2000;295(1):302-8.

Nakashima C, Ishida Y, Kitoh A, Otsuka A, Kabashima K. Interaction of peripheral nerves and mast cells, eosinophils, and basophils in the development of pruritus. Exp Dermatol 2019;28(12):1405-11.

Neher E, Sakaba T. Multiple roles of calcium ions in the regulation of neurotransmitter release. Neuron 2008;59(6):861-72.

Nelson MT, Joksovic PM, Perez-Reyes E, Todorovic SM. The endogenous redox agent L-cysteine induces T-type Ca2+ channel-dependent sensitization of a novel subpopulation of rat peripheral nociceptors. Journal of Neuroscience 2005;25(38):8766-75.

Nelson MT, Joksovic PM, Su P, Kang H-W, Van Deusen A, Baumgart JP, et al. Molecular mechanisms of subtype-specific inhibition of neuronal T-type calcium channels by ascorbate. Journal of Neuroscience 2007;27(46):12577-83.

Oetjen LK, Mack MR, Feng J, Whelan TM, Niu H, Guo CJ, et al. Sensory neurons co-opt classical immune signaling pathways to mediate chronic itch. Cell 2017;171(1):217-28. e13.

Pan H, Fatima M, Li A, Lee H, Cai W, Horwitz L, et al. Identification of a spinal circuit for mechanical and persistent spontaneous itch. Neuron 2019;103(6):1135-49. e6.

Rose KE, Lunardi N, Boscolo A, Dong X, Erisir A, Jevtovic-Todorovic V, et al. Immunohistological demonstration of CaV3. 2 T-type voltage-gated calcium channel expression in soma of dorsal root ganglion neurons and peripheral axons of rat and mouse. Neuroscience 2013;250:263-74.

Sakai K, Akiyama T. New insights into the mechanisms behind mechanical itch. Experimental dermatology 2020;29(8):680-6.

Simms BA, Zamponi GW. Neuronal voltage-gated calcium channels: structure, function, and dysfunction. Neuron 2014;82(1):24-45.

Usoskin D, Furlan A, Islam S, Abdo H, Lönnerberg P, Lou D, et al. Unbiased classification of sensory neuron types by large-scale single-cell RNA sequencing. Nature neuroscience 2015;18(1):145-53.

Wang X-L, Tian B, Huang Y, Peng X-Y, Chen L-H, Li J-C, et al. Hydrogen sulfide-induced itch requires activation of Cav3. 2 T-type calcium channel in mice. Scientific reports 2015;5(1):1-15.

Zeisel A, Hochgerner H, Lönnerberg P, Johnsson A, Memic F, Van Der Zwan J, et al. Molecular

architecture of the mouse nervous system. Cell 2018;174(4):999-1014. e22.

Figure legend.

Figure 1. Characterization of Cav3.2-expressing neurons in mouse DRGs. (a) Representative immunofluorescence images showing the expression of Cav3.2 channels in DRGs from WT and Cav3.2 knockout (KO) mice. Nuclei were stained with 4′,6-diamidino-2-phenylindole (DAPI; blue). Scale bars, 50 μm. (b) t-SNE visualization of mouse nervous system scRNA-seq profile (n = 153,633 cells) using a published dataset (Zeisel et al., 2018) showed 24 clusters. Cluster 14 is indicated with an arrow. (c) FeaturePlot showing the gene expression of itch-specific neuronal markers in a cluster 14 on a UMAP plot. (d) FeaturePlot showing the expression of genes encoding the T-type calcium channels and cell markers for three non-peptidergic (NP), tyrosine hydroxylase (TH)-positive, neurofilament (NF)-positive, and peptidergic (PEP) neurons and other itch signaling components in a cluster 14. (e) Double staining of mouse DRGs for Cav3.2 (green) and itch signaling components (red). Nuclei were stained with DAPI (blue). n=5 sections from 3 mice. Scale bars, 50 μm. (f) Percentage of Cav3.2 co-expressing neurons among mouse DRG neurons expressing TRPV1, IL-4Rα, TSLP receptor (TSLPR), or CGRP. Values presented as mean ± SEM. n=5 sections from 3 mice.

Figure 2. Expression of Cav3.2 in normal human skin.

Sections of normal human skin were double stained for pan-neuronal marker PGP9.5 (red) and Cav3.2 (green). Nuclei were stained DAPI (blue). White arrows indicate PGP9.5- and Cav3.2-immunoreactive fibers. Scale bars, 50 μm.

Figure 3. Cav3.2 channel is required for acute itch evoked by histamine, TSLP, and IL-4/IL-13. (a) WT mice were intradermally injected with mibefradil (15 μg /20 μl) or vehicle (PBS, 20 μl) into the nape of the neck and 10 minutes later injected with pruritogens, including histamine (100 μg/20μL), chloroquine (CQ) (200 μg/20 μL), PAR-2 agonist peptide (PAR2 AP) (50 μg/20μL), rmTSLP (2.5 μg/20 μL), rmIL-31 (2.5 μg/20 μL) or a combination of rmIL-4 and rmIL-13 (rmIL-4/IL-13) (1 μg/10 μL each) (n=5-6/group). PBS, phosphate-buffered saline. (b) Scratch bouts were also assessed in WT and Cav3.2 KO mice following injection of pruritogens at the nape of the neck. (n=5-6/group). The total number of scratch bouts were counted from 0 to 15 min after the injection of histamine, CQ, and PAR-2 AP or from 15 to 30 min after the injection of rmTSLP, rmIL31, and rmIL-4/IL-13 due to the different onset of scratching behavior. All data are presented as mean ± SEM. Two-tailed, unpaired Student's t-test was performed. $*P < 0.05$.

Figure 4. Increased Cav3.2 channel expression and activity contribute to increased excitability of DRG neurons in AD-like disease in mice. (a) Schematic procedure of experiments. (upper) MC903-induced AD-like model in WT mice with or without co-treatment with mibefradeil (15 μg /20 μl). (lower) Cav3.2 KO or WT littermate mice were challenged with MC903. i.d., intradermal. (b) Representative immunofluorescence images showing the expression of Cav3.2 in DRGs. Blue, DAPI-stained nuclei. Scale bars, 50 μm (left). Relative Cav3.2 mRNA expression levels in DRGs (right). n = 5 per group. Data were obtained from three independent experiments and presented as mean ± SEM. $^{**}P < 0.01$ (unpaired Student's t-test). (c) T-type calcium current density (in pA/pF) in DRG neurons of each group. n=8 mice per group. Data are shown as means ± SEM. $^{**}P < 0.01$, $^{***}P < 0.001$ by unpaired Student's t-test. (d) Effects of MC903 on the repetitive firing of action potentials (APs) in DRG neurons. AP firing number under various stimulus intensity in each group. n=8 mice per group (means ± SEM). $^{**}P < 0.01$, $^{***}P < 0.001$, vehicle control mice vs. MC903-treated mice; $^{\dagger}P < 0.05$, $^{\dagger\dagger}P < 0.01$, $^{\dagger\dagger\dagger}P < 0.001$, MC903-treated mice vs. MC903 and mibefradil-treated mice by one-way ANOVA (left). $^{**}P < 0.01$, $^{***}P < 0.001$ MC903-treated WT mice vs. MC903-treated Cav3.2 KO mice by one-way ANOVA (right). (e) AP threshold stimuli in each group. n=8 mice per group (means ± SEM). $^{*}P < 0.05$, $^{**}P < 0.01$ by unpaired Student's t-test.

Figure 5. Cav3.2 channel is required for chronic spontaneous itch and alloknesis in mouse model of AD-like inflammation. (a) Number of scratching bouts were recorded following daily application of MC903 on day 9 in WT mice with or without co-treatment with mibefradeil (15 μg /20 μl). n=11-22 mice per group. (b) Number of scratching bouts were recorded in Cav3.2 KO or littermate control mice following induction of AD-like disease by MC903 on day 9. n=15-22 mice per group. (c) Frequency of scratching bouts induced by von Frey filaments (mechanical alloknesis score) on day 9 of the MC903-AD model in WT mice with or without co-treatment with mibefradeil (15 μg /20 μl). n=10 mice per group. (d) Mechanical alloknesis score in Cav3.2 KO or littermate control mice following induction of AD-like disease by MC903 on day 9. n=10 mice per group. Data represent mean ± SEM. Two-tailed, unpaired Student's t-test was performed. $*P < 0.05$, $**P < 0.01$.

Figure 6. T-type calcium channels blockade or Cav3.2 knockout suppresses substance P and VIP production in TGs and attenuates skin inflammation in a mouse model of AD. **(a)** Representative images of MC903-treated C57BL/6 mice with or without co-treatment with mibefradil (15 μg /20 μl) and MC903-treated Cav3.2 KO mice (upper). Representative H&E- (middle) and toluidine blue-(lower) staining of each group on day 9. Scale bars, 1000 μm. Epidermal thickness (b), total immune cell counts per high-power field (HPF) (c), and mast cell counts per HPF of each group on day 9 (n=5 per group). (d) Quantitative PCR analysis of mRNA encoding cytokines in the MC903-treated neck skin of each group on day 9. Data were obtained from three independent experiments. n=5 mice per group. (e) Relative neuropeptides mRNA expression levels in trigeminal ganglia (TG)s from MC903-treated WT mice compared with vehicle control mice (n = 3~5 per group). (f) Quantitative PCR analysis of mRNA encoding neuropeptides in TGs from each group on day 9. Data were obtained from three independent experiments. n=5 mice per group. (b-f) Data are presented as mean ± SEM. Two-tailed, unpaired Student's t-test was performed. $*P < 0.05$, $**P < 0.01$, $***P < 0.001$.

Supplementary Materials and Methods

Reagents

Histamine (H7125) and chloroquine (C6628) from Sigma-Aldrich (St. Louis, MO, USA) and proteinase-activated receptor-2 agonist peptide (SLIGRL-NH2) from Peptron, Daejeon, Korea. Recombinant mouse (rm)TSLP (555-TS-010) and MC903 were purchased from R&D Systems (Minneapolis, MN, USA). rmIL-31 (210-31) and rmIL-4 (214-14) from PeproTech (Rocky Hill, NJ, USA). Mibefradil (molecular weight: 568.56) was purchased from Tocris Bioscience (Bristol, UK) and dissolved in phosphate buffered saline (PBS).

Acute itch assay

Age-matched C57BL/6 mice (Cav3.2+/+ mice) and Cana1h-/- mice (12 weeks old) were shaved on their cheeks 7 days before the experiment. On the day of the experiment, mice were individually placed in a glass chamber for at least 30 min before behavioral analysis. Histamine (100 μg/20μL), chloroquine (200 μg/20 μL), proteinase-activated receptor-2 agonist peptide (SLIGRL-NH2, 50 μg/20μL), recombinant mouse (rm) TSLP (2.5 μg/20 μL), rmIL-31 (2.5 μg/20 μL), a combination of rmIL-4 and rmIL-13 (rmIL-4/IL-13) (1 μg/10 μL each) or vehicle (PBS) was administered intradermally into the nape of the neck of mice. Scratching behavior was recorded for 30 minutes. One itch-related scratching bout was defined as an event of lifting the hind paw from the floor, scratching, and returning to the

floor. To investigate the role of TTCCs, mibefradil (15 μg /20 μl) or PBS (20 μl) was injected into the nape intradermally 10 min before the injection of pruritogens.

Histological analysis

Lesional skin of the nape of the neck was excised 24 h after the final MC903 challenge on day 9, fixed in 10% formaldehyde, and embedded in paraffin. Skin explants co-cultured with TG neurons for 24 hours were also fixed in 10% formaldehyde, and embedded in paraffin. Hematoxylin and eosin were used to stain 5-μm skin sections for inflammatory cells and with o-toluidine blue for mast cells. The stained tissues were examined under a light microscope (Olympus, Tokyo, Japan), and inflammatory or mast cells were counted in 10 random high-power fields (HPF) sections at 400× magnification. Epidermal thickness was measured using light microscopy and an eyepiece micrometer (BX-51; Olympus Corporation, Tokyo, Japan) at 100 × magnification. Each mouse (n=5) had three micrometer-scale measurements.

Immunofluorescence of mouse DRG and human skin samples

For immunofluorescence staining of mouse DRG, cervical DRGs were dissociated, fixed in fixative at 4 °C overnight, then stored in 30% sucrose in PBS at 4 °C for 3 days. The samples were embedded in an optimal cutting temperature (OCT) compound (Sakura Finetek, Tissue-Tek, PA, USA). Approximately 4μm Sections on slides were subjected to

immunofluorescence with primary antibodies, including Cav3.2 (Novus Biologicals, #NBP1-22444, 1:200), TRPV1 (Invitrogen, #PA1-29770, 1:200), IL-4Rα (Santa Cruz, #sc28361, 1:200), TSLP receptor (Prosci, #4209, 1:200), substance P (Abcam, #ab106291, 1:200), and CGRP (Abcam, ab36001, 1:200). Alexa Fluor 488 conjugated rabbit anti-mouse IgG and goat anti-human IgG (all from Thermo Fisher Scientific) were used as the secondary antibodies. Sections were stained with 4,6 diamidino 2 phenylindole (DAPI) (Thermo Fisher Scientific). For the quantification of each marker-positive neuron, 3–5 DRG sections from 3 mice were analyzed in each group.

All the studies using human skin samples were approved by the Institutional Review Board (no. IRB 3-2018-0087) of Yonsei University College of Medicine, Seoul, Korea. All donors provided written informed consent. Normal human skin samples (n = 10) were excised from patients with benign neoplasia. All donors provided written informed consent. Skin tissues from a normal individual were sectioned at 4 μm and stained with primary antibodies, including rabbit anti-human Cav3.2 antibodies (Alomone Labs, #ACC-025), and mouse anti-human PGP9.5 antibodies (Abcam, #8189, 1:200). Alexa Fluor 488 conjugated goat anti-rabbit and Alexa Flour 594 conjugated goat anti-mouse IgG antibodies (all from Thermo Fisher Scientific, 1:400) were used as the secondary antibodies. Sections were stained with DAPI (Thermo Fisher Scientific). Images were captured using an LSM 980 confocal microscope (Carl Zeiss).

Quantitative real-time RT-PCR

The quantitative real-time polymerase chain reaction was performed as previously described by our group (Kim et al., 2019). We used TaqMan probes for *Cav3.1* (Mm00486572_m1), *Cav3.2* (Mm00445359_m1), *Cav3.3* (Mm01299033_m1), *IL-4* (Mm00445259_m1), *IL-5* (Mm00439646_m1), *IL-13* (Mm00434204_m1), *TSLP* (Mm01157588_m1), *Vip* (Mm00660234_m1), *Calca* (Mm00801463_g1), *Tac1* (Mm01166996_m1), *Tac2* (Mm01160362_m1), *Adcyap1* (Mm00437433_m1), *Nppb* (Mm01255770_g1), *Npy* (Mm01410146_m1), *Nmu* (Mm00479868_m1), and *Nts* (Mm00481140_m1) (Thermo Fisher Scientific). The results were normalized to those of glyceraldehyde-3-phosphate dehydrogenase (Mm99999915_g1, GAPDH) (Thermo Fisher Scientific).

Preparation and primary culture of DRG neurons

Enzymatic methods (Chung et al., 2011) were used to dissociate DRG neurons. Briefly, animals were deeply anesthetized with isoflurane and transcardially perfused with artificial cerebrospinal fluid (CSF). DRG tissues were isolated and chopped into small pieces (Sosa et al., 1998), then incubated at 35 °C for 40 min in a shaking water bath at 120 rpm in Earle's balanced salt solution (EBSS), containing 0.6 mg/ml collagenase-type XI (Sigma-Aldrich, St.

Louis, MO) and 0.3 mg/ml Papain (Sigma-Aldrich, St. Louis, MO), After enzymatic digestion, ganglionic tissues were triturated into single neurons using fire-polished wide-bore Pasteur pipettes in multiple steps. After 1000 rpm centrifugation, cells were resuspended in Dulbecco's modified Eagle's medium (DMEM) containing 10% fetal bovine serum (FBS) and 1% penicillin/streptomycin (Invitrogen, USA). The resuspended cells were seeded onto poly L-lysine-coated 12-mm glass coverslips and incubated in a humidified incubator with 95% air and 5% CO_2. The neurons were used within 12 h of plating.

Electrophysiology

Voltage-gated Ca2+ currents (ICa) were measured using conventional whole-cell techniques. When filled with an internal solution, the electrode resistances were 3–5 mΩ. The patch-clamp amplifier Axopatch 200A (Molecular Devices) was used for the measurements. The Digidata 1322A interfaced with Clampex 9.2 (pClamp Software, Molecular Devices, USA) on an IBM-compatible computer was used to control voltage and current commands and the digitization of membrane voltages and currents. Clampfit (Molecular Devices, USA) and Prism 9.0 (GraphPad, USA) were used to analyze the data. A DRG-seeded cover glass was placed in a recording chamber with saline solution perfusion (pH 7.4). Currents were low-pass filtered at 2 kHz using the four-pole Bessel filter of the amplifier. pClamp software automatically calculated capacitance (Cm) values during recordings. The clamp mode

recorded action potential. Membrane potential measurements were low-pass filtered at 10 kHz. Only cells with a resting membrane potential ≤ 50mV were analyzed. A gravity-driven fast drug perfusion system uses multiple independently controlled syringes as reservoirs. Switching between solutions was accomplished by manually controlled valves. All experiments were performed at room temperature. The external solution used for current-clamp recordings contained 145 mM NaCl, 5.4 mM KCl, 2.5 mM CaCl2, 1.2 mM MgCl2, 10 mM glucose and 10 mM HEPES; the solution was adjusted to pH 7.4 with NaOH. The pipette solution used for current-clamp recordings contained 113 mM K-gluconate, 30 mM KCl, 1.2 mM MgCl2, 4 mM MgATP, 0.4 mM Na2GTP, 10 mM phosphocreatine, 10 mM HEPES, and 0.05 mM EGTA; the solution was adjusted to pH 7.2 with KOH. Actional potentials were evoked by constant-current injection of positive currents (10 – 70 pA) for 900 ms in the current-clamp mode.

Ex vivo co-culture experiments

TG neurons were obtained from the ethanol-treated wild-type (WT) mice, MC903-treated WT mice, and MC903-treated Cav3.2 knockout mice 24 hours after the final ethanol or MC903 challenge on day 9 (n= 6 mice per group). Twelve TG neurons obtained from each group (left and right TGs from each mouse) were divided into three wells of a 24-well plate containing 2ml of 10% DMEM, with 4 TG samples each. Additionally, twelve skin explants

obtained from the back skin of an 8-week-old normal mouse using a 2mm punch were added to each well. In each well, four TG neurons and twelve pieces of 2mm punch-excised skin explants were fully submerged in the media and co-cultured for 24 hours. After co-culture, two skin specimens per each well were fixed in neutrally buffered 4% formaldehyde and embedded in paraffin and the rest skin specimens were stored for real-time RT-PCR. The culture media was aliquoted into 110µl and stored in a deep freezer until further analysis for ELISA.

ELISA

The protein expression levels of substance P and VIP secreted into the supernatants of ex vivo co-culture of TG neurons and skin explants were quantified in triplicate via ELISA kits for substance P (R&D systems, #KGE007) and VIP (Cusabio Technology LLC, # CSBE08354h) following the manufacturer's instructions.

Western blotting

Total proteins from mouse brain, mouse TG neurons, mouse epidermis, mouse dermis, and primary human keratinocytes were isolated using RIPA buffer (Cell Signaling Technology, Danvers, MA) supplemented with protease inhibitor cocktail (sigma Aldrich, #8340). After protein isolation, equal amounts of proteins from each group were loaded onto Nupage 3-8%

Tris-acetate Gels (Thermo Fisher Scientific, #EA0375BOX), and electrophoresis was performed using an X-cell SureLock Mini-Cell (Thermo Fisher Scientific). After electrophoresis, proteins were transferred onto polyvinylidene difluoride membranes, which were then incubated with rabbit polyclonal anti-Cav3.2 antibody (Novus biologicals, #NBP1-22444) that was diluted in Tris-buffered saline (TBS) containing 0.05% Tween 20 (TBS-T), at a dilution of 1:2000. Blots were washed with 0.05% TBS-T and then incubated with horseradish peroxidase-conjugated anti-mouse secondary antibodies (Invitrogen, #62-6520) in 0.05% TBS-T at a dilution of 1:3000. Blots were developed using NovexTM ECL Chemiluminescent Substrate reagent Kit (Invitrogen, #WP20005).

Supplementary Figure legends

Supplementary Figure S1. Validation of the specificity of antibodies used in the immunofluorescence experiments. (a) Negative control staining was performed by omitting the primary antibodies against Cav3.2 in DRG from WT and Cav3.2 knockout (KO) mice. Nuclei were stained with 4′,6-diamidino-2-phenylindole (DAPI; blue). Scale bars, 50 μm. (b) Negative control staining was performed by omitting the primary antibodies against Cav3.2 and TRPV1, Cav3.2 and IL-4Rα, Cav3.2 and TSLPR, or Cav3.2 and CGRP in DRG from WT mice. Nuclei were stained with DAPI. Scale bars, 50 μm. Rb, rabbit; Ms, mouse; GP, guinea pig.

Supplementary Figure S2. Administration of the T-type calcium channels (TTCCs) blocker, mibefradil, induces a dose-dependent attenuation in skin inflammation in MC903-induced AD-like mice. (a) Representative images of MC903-treated C57BL/6 mice co-treated with mibefradil at doses of 1.2 μg/20 μl, 15 μg/20 μl, or 35 μg/20 μl (n=4-5 mice per dose group) via two days of topical and four days of intradermal administration (as illustrated in Figure 4a), along with the corresponding vehicle control. (b) Representative H&E staining of each group on day 9. Scale bars, 200 μm. (c) Epidermal thickness of each group on day 9. (d) Quantitative PCR analysis of mRNA encoding cytokines in the MC903-treated neck skin of each group on day 9. Data were obtained from three independent experiments (mean ± SEM). n=4-5 mice per group. Two-tailed, unpaired Student's t-test was performed. $*P < 0.05$, $**P < 0.01$. $^{\#}P<0.05$ and $^{\#\#}P<0.01$ versus the vehicle control group. Mibe, mibefradil.

Supplementary Figure S3. Expression of Cav3.2 in mouse TG neurons but not in mouse epidermis and human keratinocytes. (a) Quantitative PCR analysis of Cav3 channels (Cav3.1, Cav3.2, and Cav3.3) mRNA expression in mouse brain, mouse DRG neurons, mouse TG neurons, and mouse epidermis. Results are normalized to the internal control GAPDH and are shown relative to those in mouse brain. Data are expressed as mean ± SEM of three independent

experiments. (b) Expression levels of Cav3.2 in mouse brain, mouse TG neurons, mouse epidermis, mouse dermis, and human keratinocytes were examined by Western blot. GAPDH, glyceraldehyde-3-phosphate; n.d., not detected.

Supplementary Figure S4. Effect of the addition of TG neurons from MC903-treated wild-type or Cav3.2 knockout mice on normal mouse skin explants in an ex vivo co-culture system. (a) Quantitative analysis of neuropeptide levels in the culture medium of TG neurons from ethanol-treated wild-type (WT) mice (WT controls), MC903-treated WT mice (WT MC903), or MC903-treated Cav3.2 knockout mice (Cav3.2 KO MC903) using ELISA assay. Data were obtained from three independent experiments (mean ± SEM). n=6 mice per group. (b) Co-culture of TG neurons from MC903-treated WT mice with normal skin explants induces epidermal hyperplasia and dermal inflammatory infiltrates. These changes are attenuated in skin explants co-cultured with MC903-treated Cav3.2 knockout mice. Representative H&E staining of each group after 24 hours of co-culture. Scale bars, 200 μm. (c) Epidermal thickness of each group after 24 hours of co-culture. (d) Quantitative PCR analysis of mRNA encoding cytokines in the skin explants co-cultured with TGs from MC903-treated WT or Cav3.2 knockout mice. Data were obtained from three independent experiments (mean ± SEM). Two-tailed, unpaired Student's t-test was performed. *$P < 0.05$, **$P < 0.01$.

Supplementary References

Chung S, Kim YH, Koh JY, Nam TS, Ahn DS. Intracellular acidification evoked by moderate extracellular acidosis attenuates transient receptor potential V1 (TRPV1) channel activity in rat dorsal root ganglion neurons. Experimental Physiology 2011;96(12):1270-81.

Kim JH, Kim SE, Park HS, Lee SH, Lee SE, Kim SC. A homozygous nonsense mutation in the DSG3 gene causes acantholytic blisters in the oral and laryngeal mucosa. Journal of Investigative Dermatology 2019;139(5):1187-90.

Sosa IJ, Reyes O, Inserni J, Kuffler DP. Isolation and long-term survival of adult human sensory neurons in vitro. Neurosurgery 1998;42(3):681-6.

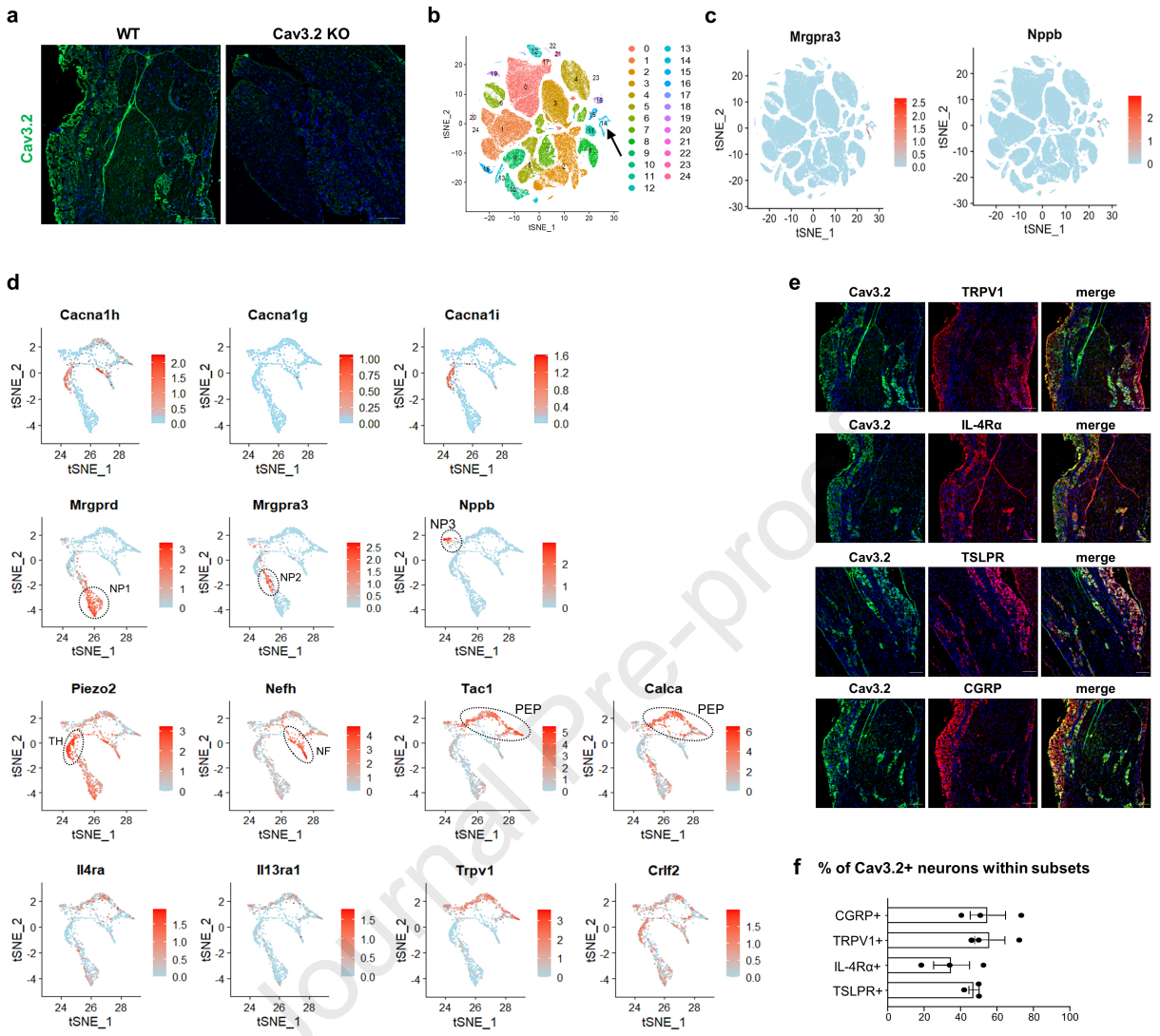
a
WT
Cav3.2 KO
Cav3.2
b
c
Mrgpra3
Nppb
d
Cacna1h
Cacna1g
Cacna1i
Mrgprd
Mrgpra3
Nppb
NP1
NP2
NP3
Piezo2
Nefh
Tac1
Calca
TH
NF
PEP
Il4ra
Il13ra1
Trpv1
Crlf2
tSNE_1
tSNE_2
e
Cav3.2
TRPV1
merge
IL-4Rα
TSLPR
CGRP
f
% of Cav3.2+ neurons within subsets
CGRP+
TRPV1+
IL-4Rα+
TSLPR+

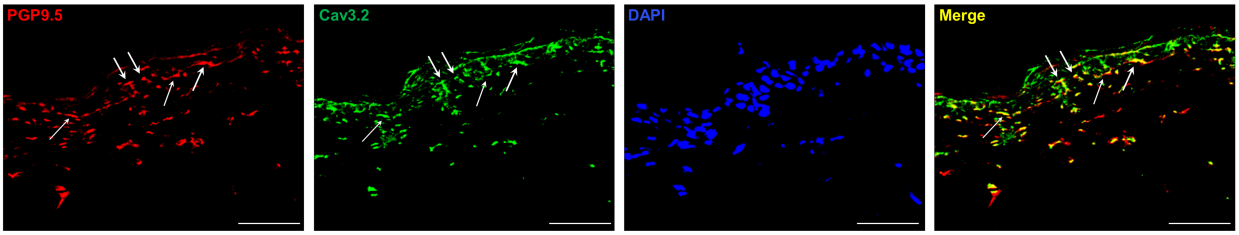

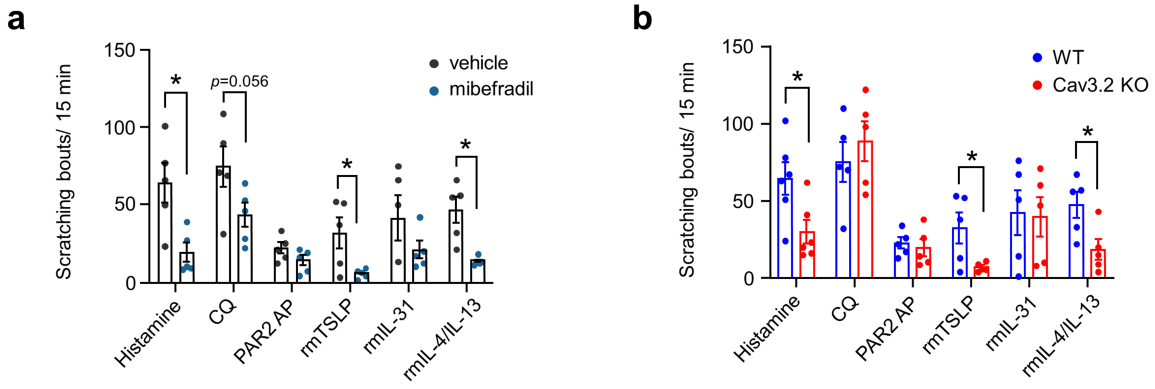

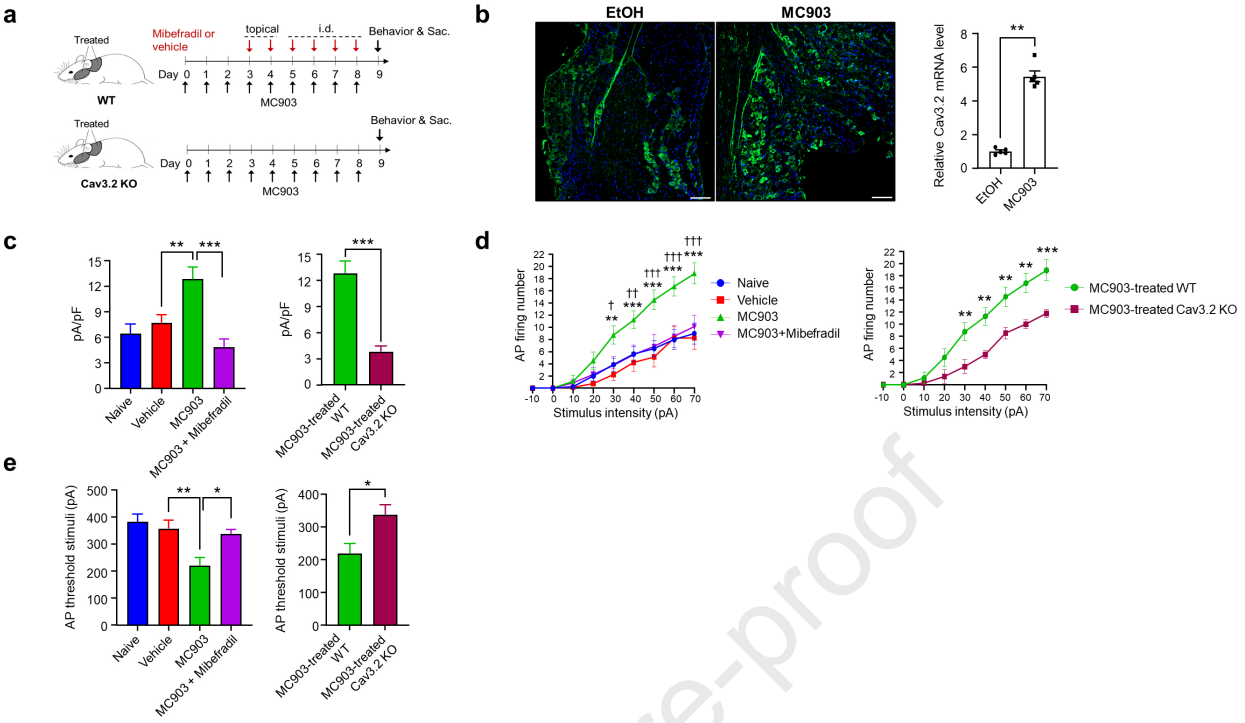

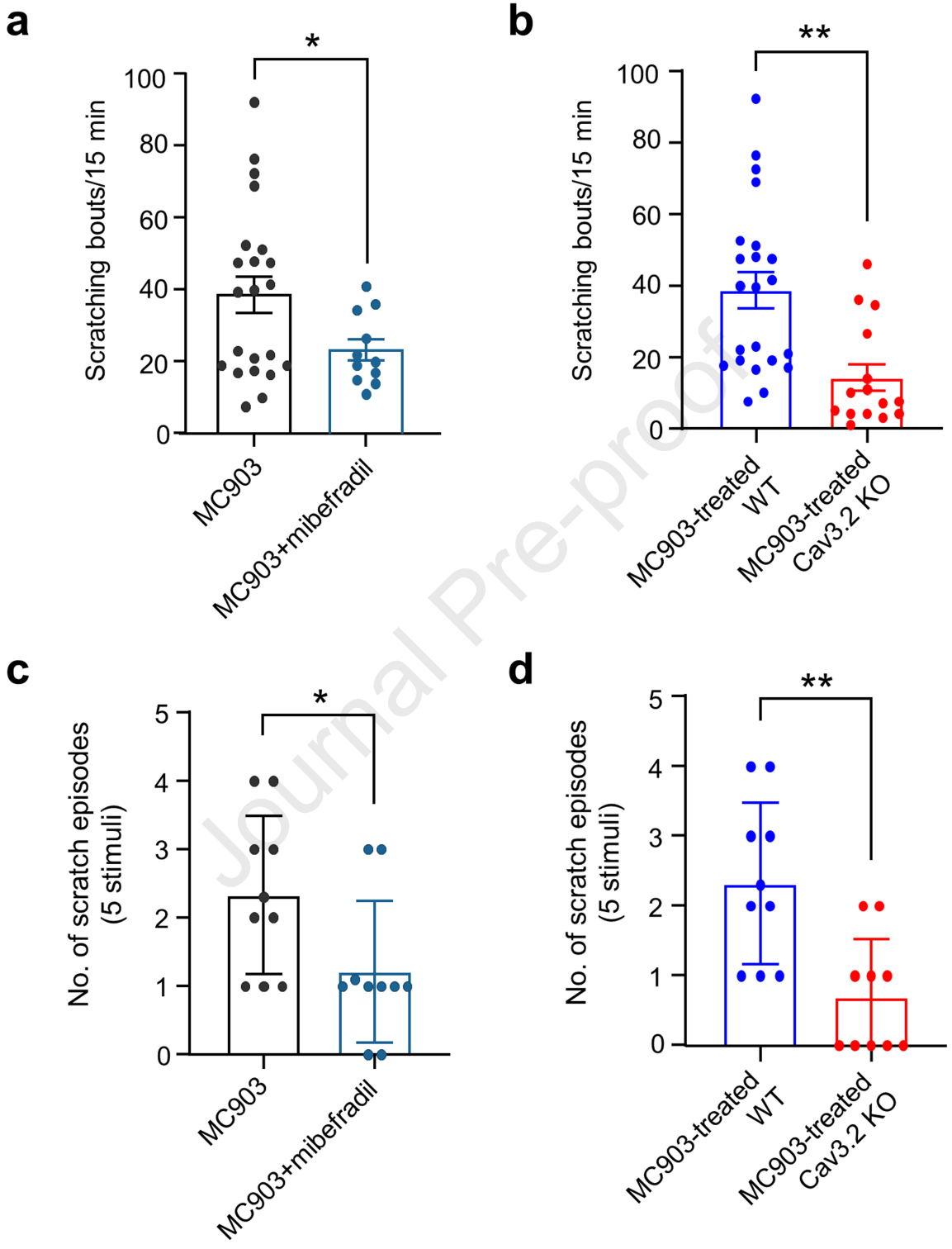

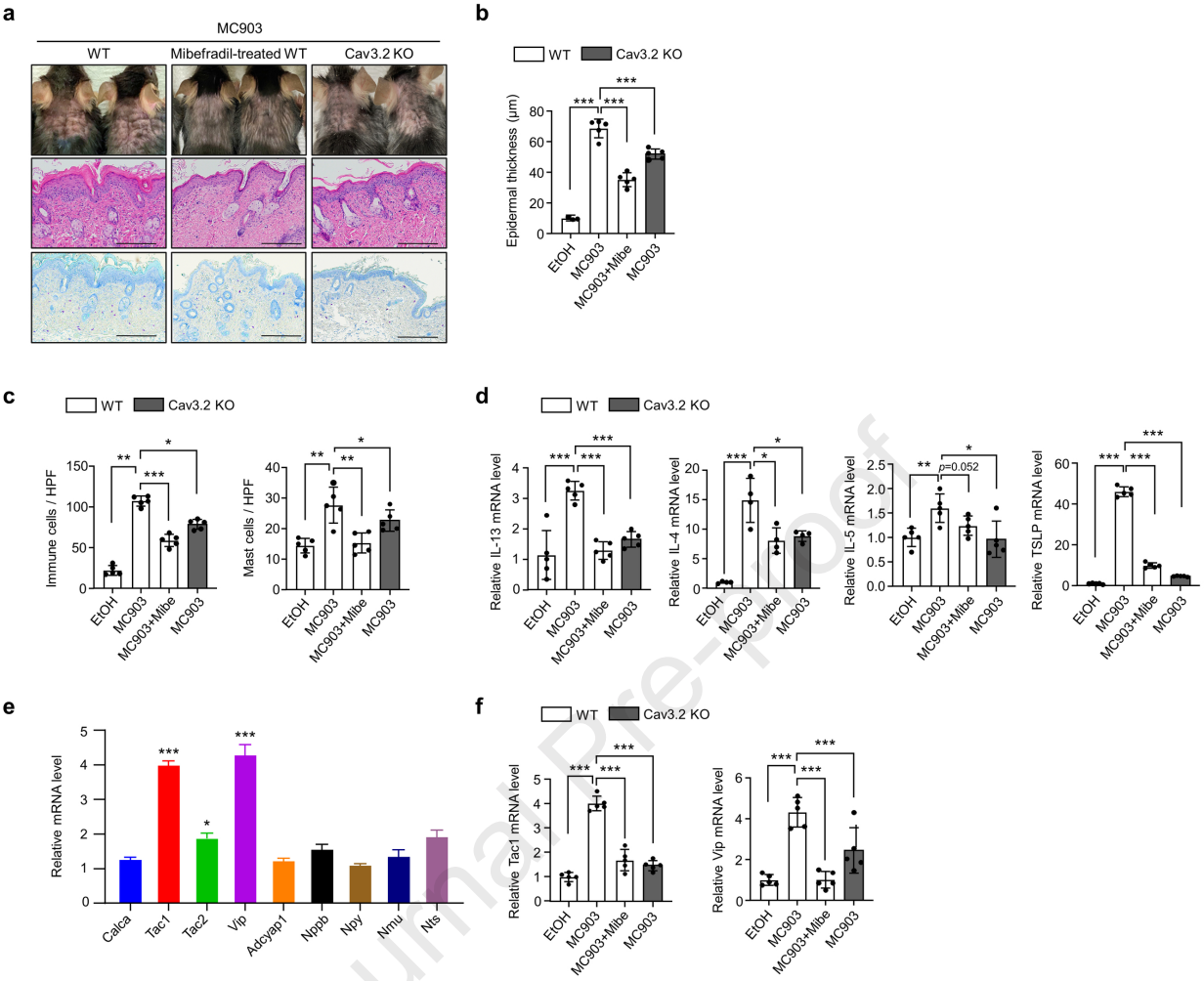

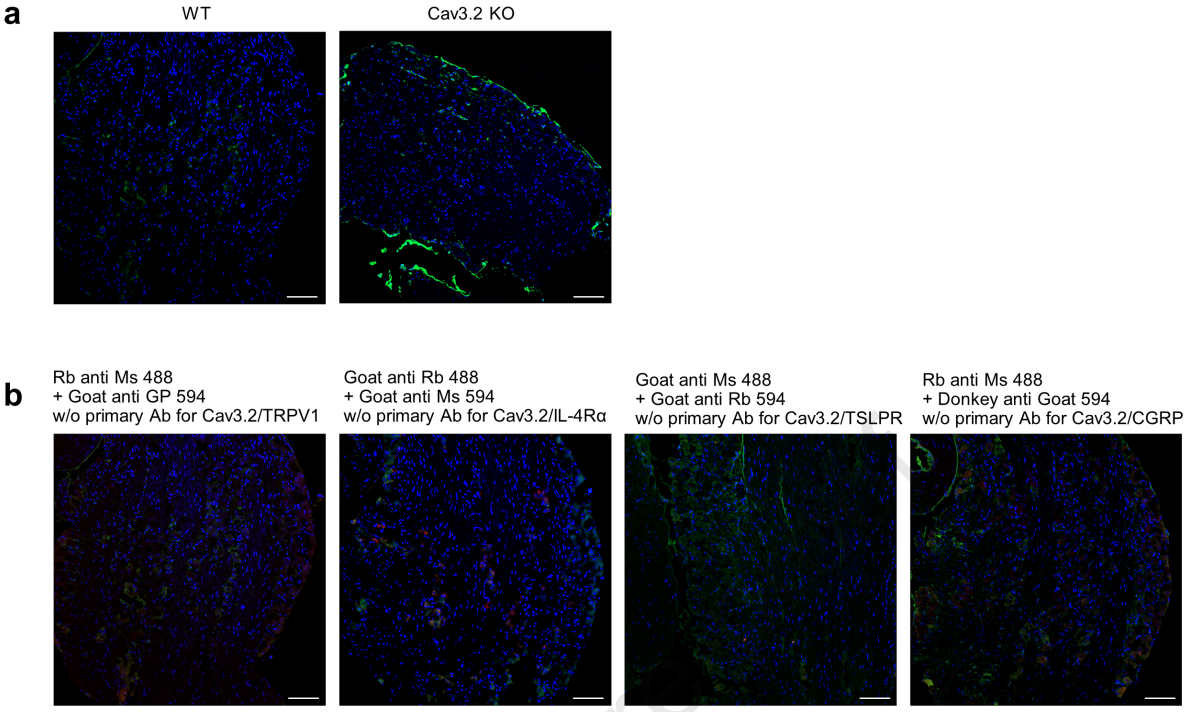

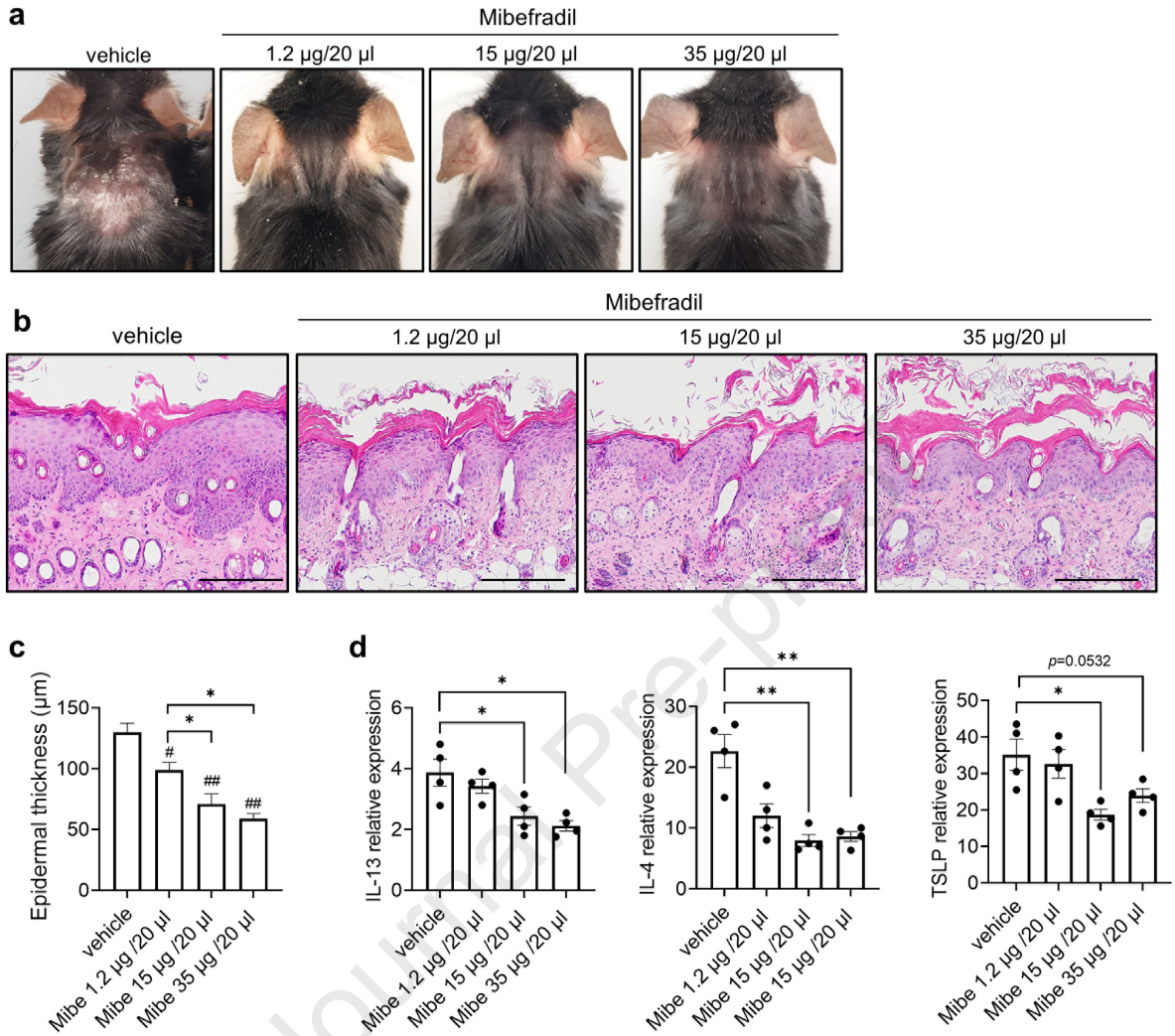
a
Mibefradil
vehicle
1.2 μg/20 μl
15 μg/20 μl
35 μg/20 μl
b
Mibefradil
vehicle
1.2 μg/20 μl
15 μg/20 μl
35 μg/20 μl
c
Epidermal thickness (μm)
150
100
50
0
*
*
#
##
##
vehicle
Mibe 1.2 μg /20 μl
Mibe 15 μg /20 μl
Mibe 35 μg /20 μl
d
IL-13 relative expression
6
4
2
0
*
*
vehicle
Mibe 1.2 μg /20 μl
Mibe 15 μg /20 μl
Mibe 35 μg /20 μl
IL-4 relative expression
30
20
10
0
**
**
vehicle
Mibe 1.2 μg /20 μl
Mibe 15 μg /20 μl
Mibe 15 μg /20 μl
TSLP relative expression
p=0.0532
50
40
30
20
10
0
*
vehicle
Mibe 1.2 μg /20 μl
Mibe 15 μg /20 μl
Mibe 35 μg /20 μl